11th AIAA/ASME Joint Thermophysics and Heat Transfer Conference, AIAA Aviation and Aeronautics Forum and Exposition 2014,
16 - 20 June 2014, Atlanta, Georgia, USA

# The effect of noncondensables on thermocapillary-buoyancy convection in volatile fluids

Tongran Qin*
*George W. Woodruff School of Mechanical Engineering, Georgia Institute of Technology*
*Atlanta, GA, 30332-0405, USA*
Roman O. Grigoriev†
*School of Physics, Georgia Institute of Technology*
*Atlanta, GA, 30332-0430, USA*

**Convection in confined layers of volatile liquids has been studies extensively under atmospheric conditions. Recent experimental results[1] have shown that removing most of the air from a sealed cavity significantly alters the flow structure and, in particular, suppresses transitions between different convection patterns found at atmospheric conditions. To understand these results, we have formulated and numerically implemented a detailed transport model that accounts for mass and heat transport in both phases as well as the phase change at the interface. Numerical simulations show that, rather unexpectedly, noncondensables have a large effect on not only the buoyancy-thermocapillary flow at concentrations as low as one percent (which is much lower than those achieved in experiment), but also the transitions between the different flow patterns.**

## Nomenclature

| | | | |
|---|---|---|---|
| $\alpha$ | Thermal Diffusivity | $m$ | Mass |
| $\beta$ | Coefficient of Thermal Expansion | $M$ | Molar Mass |
| $\gamma$ | Temperature Coefficient of Surface Tension | $Ma$ | Marangoni Number |
| $\mu$ | Dynamic Viscosity | $p$ | Pressure |
| $\rho$ | Density | $p_0$ | Pressure Offset |
| $\kappa$ | Interfacial Curvature | $Pr$ | Prandtl Number |
| $\sigma$ | Surface Tension | $R$ | Universal Gas Constant |
| $\lambda$ | Accommodation Coefficient | $\bar{R}$ | Specific Gas Constant |
| $\tau$ | Interfacial Temperature Gradient | $Ra$ | Rayleigh Number |
| $\Sigma$ | Stress Tensor | $t$ | Time |
| $Bo_D$ | Dynamic Bond Number | $T$ | Temperature |
| $c$ | Mole Fraction | $T_0$ | Ambient Temperature |
| $\bar{c}$ | Average Mole Fraction | $\Delta T$ | Applied Temperature Difference |
| $c_p$ | Heat Capacity | $\mathbf{u}$ | Velocity |
| $D$ | Binary Mass Diffusion Coefficient | $V$ | Volume |
| $d_l$ | Liquid Layer Thickness | $x, y, z$ | Coordinate Axes |

*Ph.D. student, Mechanical Engineering, Georgia Institute of Technology, 771 Ferst Dr. NW, Atlanta, GA 30332-0405 USA, Student Member.
†Associate Professor, Physics, Georgia Tech, 837 State Street, Atlanta, GA 30332-0430 USA

| | | | |
|---|---|---|---|
| $g$ | Gravitational Acceleration | *Subscript* | |
| $h_w$ | Wall Thickness | $l$ | Liquid Phase |
| $J$ | Mass Flux Across the Liquid-Gas Interface | $g$ | Gas Phase |
| $k$ | Thermal Conductivity | $v$ | Vapor Component |
| $\mathcal{L}$ | Latent Heat of Vaporization | $a$ | Air Component |
| $L, W, H$ | Test Cell Dimensions | $i$ | Liquid-Gas Interface |
| | | $s$ | Saturation |
| *Superscript* | | $c$ | Cold End |
| $*$ | Reference Value | $h$ | Hot End |

# I. Introduction

Convection in a layer of fluid with a free surface due to a combination of thermocapillary stresses and buoyancy has been studied extensively due to applications in thermal management in terrestrial environments. In particular, devices such as heat pipes and heat spreaders, which use phase change to enhance thermal transport, are typically sealed, with noncondensables (such as air), which can impede phase change, removed.[2] However, because noncondensables tend to dissolve in liquids, is impossibly to remove them entirely. Hence, the vapor phase almost always contains a mixture of vapor and air. The fundamental studies on which the design of thermal management devices is based, however, often do not distinguish between different compositions of the gas phase. On the other hand, the experimental studies are typically performed in geometries that are not sealed and hence contain air at atmospheric pressure, while most theoretical studies ignore phase change completely. Those that do consider phase change use transport models of the gas phase that are too crude to properly describe the effect of noncondensables on the flow in the liquid layer. Yet, as a recent experimental study by Li *et al.*[1] shows, noncondensables play an important and nontrivial role, so the results in one limit cannot be simply extrapolated to the other.

We have recently introduced a comprehensive two-sided model[3] for buoyancy-thermocapillary convection in confined fluids which provides a detailed description of momentum, heat and mass transport in both the liquid and the gas phase as well as phase change at the interface. In the limit where the system is at ambient (atmospheric) conditions, this model shows that at dynamic Bond numbers $Bo_D = O(1)$, the flow in the liquid layer transitions from a steady unicellular pattern (featuring one big convection roll) to a steady multicellular pattern (featuring multiple steady convection rolls) to an oscillatory pattern (featuring multiple unsteady convection rolls) as the applied temperature gradient is increased, which is consistent with previous experimental studies of volatile and nonvolatile fluids,[1,4–7] as well as previous numerical studies of nonvolatile fluids.[4,8–11]

In comparison, very few studies have been performed in the (near) absence of noncondensables. In partricular, the theoretical studies[12–16] employ extremely restrictive assumptions and/or use a very crude description of one of the two phases. We are not aware of any theoretical studies of the intermediate case when the fractions of vapor and noncondensables are similar, which is the situation most relevant for thermal management applications. As the experiments of Li *et al.*[1] performed for a volatile silicone oil at dynamic Bond numbers $Bo_D \approx 0.7$ demonstrate, transitions between different convection patterns are delayed as the fraction of air is decreased. On the other hand, the structure of the base (i.e., unicellular) flow remains essentially the same even when the fraction of noncondensables is reduced to around 10%, which corresponds to a reduction of the total pressure by two orders of magnitude, compared with atmospheric.

To better understand the effect of noncondensables on the transitions between different flow patterns, we have modified our two-sided model[3,17] to describe the limit in which the gas phase is dominated by vapor, rather than noncondensables. This updated model enables us to both understand the experimental results of Li *et al.*[1] and make a connection to our previous analysis of convection under pure vapor.[17] The model is described in detail in Section II. Results of the numerical investigations are presented, analyzed, and compared with experimental findings in Section III. Finally, Section IV presents our conclusions.

# II. Mathematical Model

Due to the lack of a computationally tractable generalization of the Navier-Stokes equation for multicomponent mixtures, we are restricted to situations where the dilute approximation is valid in the gas phase,

e.g., when the molar fraction of one component is much greater than that of the other. Hence, in order to explore a wider range of molar fractions, we use two different versions of the transport model. The limit where the gas phase is dominated by noncondensables is described using the model introduced for convection under atmospheric conditions.[3] To describe the opposite limit, where vapor dominates, we introduce below a generalization of the model that was originally developed for convection under pure vapor.[17]

### A. Governing Equations

Both the liquid and the gas phase are considered incompressible and the momentum transport in the bulk is described by the Navier-Stokes equation

$$\rho\left(\partial_t \mathbf{u} + \mathbf{u}\cdot\nabla\mathbf{u}\right) = -\nabla p + \mu\nabla^2\mathbf{u} + \rho\left(T\right)\mathbf{g} \tag{1}$$

where $p$ is the fluid pressure, $\rho$ and $\mu$ are the fluid's density and viscosity, and $\mathbf{g}$ is the gravitational acceleration.

Following standard practice, we use the Boussinesq approximation, retaining the temperature dependence only in the last term to represent the buoyancy force. In the liquid phase

$$\rho_l = \rho_l^*[1 - \beta_l\left(T - T^*\right)], \tag{2}$$

where $\rho_l^*$ is the reference density at the reference temperature $T^*$ and $\beta_l = -(\partial\rho_l/\partial T)/\rho_l$ is the coefficient of thermal expansion. Here and below, subscripts $l$, $g$, $v$, $a$ and $i$ denote properties of the liquid and gas phase, vapor and air component, and the liquid-gas interface, respectively. In the gas phase

$$\rho_g = \rho_a + \rho_v, \tag{3}$$

where both vapor ($n = v$) and air ($n = a$) are considered to be ideal gases

$$p_n = \rho_n \bar{R}_n T, \tag{4}$$

$\bar{R}_n = R/M_n$, $R$ is the universal gas constant, and $M_n$ is the molar mass. The total gas pressure is the sum of partial pressures

$$p_g = p_a + p_v. \tag{5}$$

On the left-hand-side of (1) the density is considered constant for each phase (defined as the spatial average of $\rho(T)$).

For a volatile fluid in confined geometry, the external temperature gradient causes both evaporation and condensation, with the net mass of the fluid being globally conserved. The mass transport of the less abundant component is described by the advection-diffusion equations for its density to ensure local mass conservation. When vapor dominates, the less abundant component is air, so we have

$$\partial_t \rho_a + \mathbf{u}\cdot\nabla\rho_a = D\nabla^2\rho_a, \tag{6}$$

where $D$ is the binary diffusion coefficient of air in vapor. Mass conservation for the liquid and its vapor requires

$$\int_{\text{liquid}} \rho_l dV + \int_{\text{gas}} \rho_v dV = m_{l+v}, \tag{7}$$

where $m_{l+v}$ is the total mass of liquid and vapor. The total pressure in the gas phase is $p_g = p + p_o$, where the pressure offset $p_o$ is

$$p_o = \left[\int_{\text{gas}} \frac{1}{\bar{R}_v T} dV\right]^{-1} \left[m_{l+v} - \int_{\text{liquid}} \rho_l dV - \int_{\text{gas}} \frac{p}{\bar{R}_v T} dV\right]. \tag{8}$$

The concentrations of the two components (defined as molar fractions) can be computed from the equation of state using the partial pressures

$$c_n = p_n/p_g. \tag{9}$$

Finally, the transport of heat is also described by an advection-diffusion equation

$$\partial_t T + \mathbf{u}\cdot\nabla T = \alpha\nabla^2 T, \tag{10}$$

where $\alpha = k/\rho c_p$ is the thermal diffusivity, $k$ is the thermal conductivity, and $c_p$ is the heat capacity, of the fluid.

## B. Boundary Conditions

The system of coupled evolution equations for the velocity, pressure, temperature, and density fields has to be solved in a self-consistent manner, subject to the boundary conditions describing the balance of momentum, heat, and mass fluxes. The phase change at the liquid-gas interface can be described using Kinetic Theory.[18] The mass flux across the interface is given by[19]

$$J = \frac{2\lambda}{2-\lambda}\,\rho_v\sqrt{\frac{\bar{R}_v T_i}{2\pi}}\left[\frac{p_l - p_g}{\rho_l \bar{R}_v T_i} + \frac{\mathcal{L}}{\bar{R}_v T_i}\frac{T_i - T_s}{T_s}\right], \tag{11}$$

where $\lambda$ is the accommodation coefficient, which is usually taken to be equal to unity (the convention we follow here) and subscript $s$ denotes saturation values for the vapor. The dependence of the local saturation temperature on the partial pressure of vapor is described using the Antoine's equation for phase equilibrium

$$\ln p_v = A_v - \frac{B_v}{C_v + T_s} \tag{12}$$

where $A_v$, $B_v$, and $C_v$ are empirical coefficients.

Mass flux balance on the gas side of the interface is given by

$$J = -D\,\mathbf{n}\cdot\nabla\rho_v + \rho_v\,\mathbf{n}\cdot(\mathbf{u}_g - \mathbf{u}_i), \tag{13}$$

where the first term represents the diffusion component, and the second term represents the advection component (referred to as the "convection component" by Wang *et al.*[20]) and $\mathbf{u}_i$ is the velocity of the interface. Since air is noncondensable, its mass flux across the interface is zero, therefore

$$0 = -D\,\mathbf{n}\cdot\nabla\rho_a + \rho_a\,\mathbf{n}\cdot(\mathbf{u}_g - \mathbf{u}_i). \tag{14}$$

For binary diffusion, the diffusion coefficient of vapor in air is the same as that of air in vapor, while the concentration gradients of vapor and air have the same absolute value but opposite direction, which yields the relation between the density gradients of vapor and air

$$\bar{R}_v T_i^2\,\mathbf{n}\cdot\nabla\rho_v + \bar{R}_a T_i^2\,\mathbf{n}\cdot\nabla\rho_a = -p_g\,\mathbf{n}\cdot\nabla T_g, \tag{15}$$

Finally, the heat flux balance is given by

$$\mathcal{L}J = \mathbf{n}\cdot k_l\nabla T_l - \mathbf{n}\cdot k_g\nabla T_g. \tag{16}$$

The remaining boundary conditions for $\mathbf{u}$ and $T$ at the liquid-vapor interface are standard: the temperature is considered to be continuous

$$T_l = T_i = T_v \tag{17}$$

and so are the tangential velocity components

$$(1 - \mathbf{n}\cdot\mathbf{n})(\mathbf{u}_l - \mathbf{u}_g) = 0. \tag{18}$$

The normal component of $\mathbf{u}_l$ is computed using mass balance across the interface. Furthermore, since the liquid density is much greater than that of the gas,

$$\mathbf{n}\cdot(\mathbf{u}_l - \mathbf{u}_i) = \frac{J}{\rho_l} \approx 0. \tag{19}$$

The stress balance

$$(\Sigma_l - \Sigma_g)\cdot\mathbf{n} = \mathbf{n}\kappa\sigma - \gamma\nabla_s T_i \tag{20}$$

incorporates both the viscous drag between the two phases and thermocapillary effects. Here

$$\Sigma = \mu\left[\nabla\mathbf{u} - (\nabla\mathbf{u})^T\right] - p \tag{21}$$

is the stress tensor, $\kappa$ is the interfacial curvature, $\nabla_s = (1-\mathbf{n}\cdot\mathbf{n})\,\nabla$ is the surface gradient and $\gamma = -\partial\sigma/\partial T$ is the temperature coefficient of surface tension.

We use Newton iteration to solve for the mass flux $J$, the interfacial temperature $T_i$, the saturation temperature $T_s$, the normal component of the gas velocity at the interface $\mathbf{n}\cdot\mathbf{u}_g$, the density of the dominant component in the gas phase and the normal component of the density gradient of the less abundant component on the gas side (air at reduced pressures, vapor at atmospheric pressures).

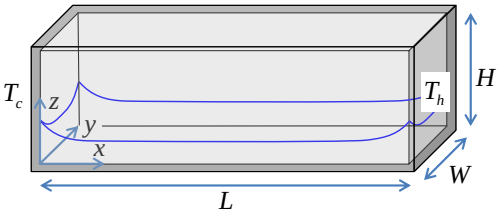


**Figure 1. The test cell containing the liquid and air/vapor mixture. Gravity is pointing in the negative $z$ direction. The inner dimensions of the cell are $L \times H \times W = 48.5$ mm $\times 10$ mm $\times 10$ mm.**

We further assume that the fluid is contained in a rectangular test cell with inner dimensions $L \times W \times H$ (see Fig. 1) and thin walls of thickness $h_w$ and conductivity $k_w$. The left wall is cooled with constant temperature $T_c$ imposed on the outside, while the right wall is heated with constant temperature $T_h > T_c$ imposed on the outside. Since the walls are thin, one-dimensional conduction is assumed, yielding the following boundary conditions on the inside of the side walls:

$$T|_{x=0} = T_c + \frac{k_n}{k_w} h_w \, \mathbf{n}\cdot\nabla T, \tag{22}$$

$$T|_{x=L} = T_h + \frac{k_n}{k_w} h_w \, \mathbf{n}\cdot\nabla T, \tag{23}$$

where $n = g$ ($n = l$) above (below) the contact line.

Heat flux through the top, bottom, front and back walls is ignored (adiabatic boundary conditions are typical of most experiments). Standard no-slip boundary conditions $\mathbf{u} = 0$ for the velocity and no-flux boundary conditions

$$\mathbf{n}\cdot\nabla\rho_n = 0 \tag{24}$$

for the density of the less abundant component ($n = a$ or, at atmospheric conditions, $n = v$), are imposed on all the walls. The pressure boundary condition

$$\mathbf{n}\cdot\nabla p = \rho(T)\,\mathbf{n}\cdot\mathbf{g} \tag{25}$$

follows from (1).

## III. Results and Discussion

The model described above has been implemented numerically by adapting an open-source general-purpose CFD package OpenFOAM[21] to solve the governing equations in both 2D and 3D geometries. The details can be found in our earlier paper.[3] The model is used in this study to investigate the buoyancy-thermocapillary flow of 0.6 cSt silicone oil (its material properties are summarized in Table 1) under conditions mostly similar of the experimental study of Li *et al.*[1]

| | liquid | vapor | air |
|---|---|---|---|
| $\mu$ (kg/(m·s)) | $4.95 \times 10^{-4}$ | $6.0 \times 10^{-6}$ | $1.82 \times 10^{-5}$ |
| $\rho$ (kg/m$^3$) | 761.0 | 0.275 | $p_a/(\bar{R}_a T_0)$ |
| $\beta$ (1/K) | $1.34 \times 10^{-3}$ | $1/T$ | |
| $k$ (W/(m·K)) | 0.1 | 0.03 | 0.03 |
| $\alpha$ (m$^2$/s) | $9.52 \times 10^{-8}$ | $9.08 \times 10^{-5}$ | $1.89 \times 10^{-5}$ |
| $Pr$ | 6.83 | 0.24 | 0.67 |
| $\sigma$ (N/m) | $1.59 \times 10^{-2}$ | | |
| $\gamma$ (N/(m·K)) | $7 \times 10^{-5}$ | | |
| $D$ (m$^2$/s) | $2.5 \times 10^{-5}$ | | |
| $\mathcal{L}$ (J/kg) | $2.14 \times 10^5$ | | |

**Table 1. Material properties of hexamethyldisiloxane at the reference temperature $T_0 = 293$ K. In the gas phase, based on the ideal-gas assumption, the average value of the density of air $\rho_a = p_a/(\bar{R}_a T_0)$, the coefficient of thermal expansion $\beta = 1/T$, and the viscosity is taken equal to that of the dominant component.**

The are several differences. First of all, silicone oil wets the walls of the container (made from fuzed quartz) very well, so the contact angle is quite small. In this study we set the contact angle $\theta = 90°$ to avoid numerical instabilities and reduce computational resources. This has a minor effect on the shape of the free surface everywhere except very near the contact lines; moreover, previous studies[3] show that the

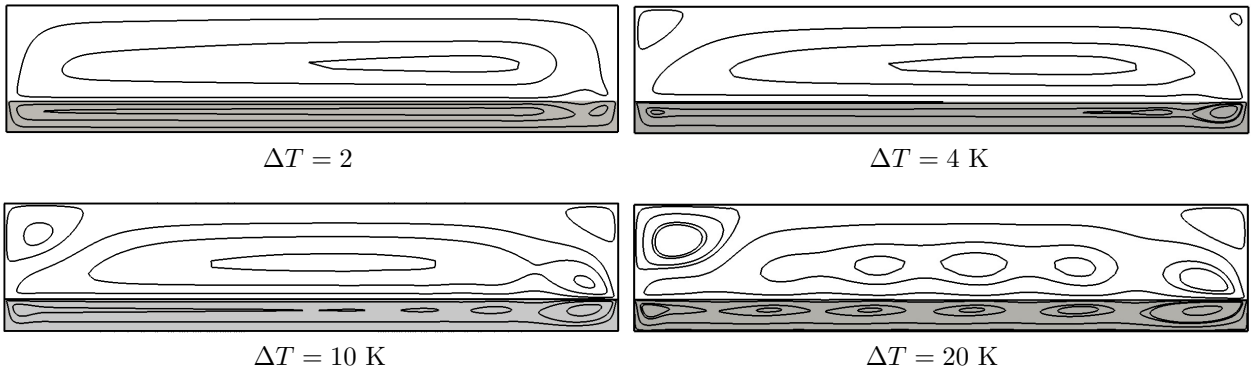


**Figure 2. Flow patterns at atmospheric conditions ($\bar{c}_a = 0.96$). Here and below, solid lines represent the streamlines of the flow and the gray (white) background indicates the liquid (gas) phase.**

flow pattern depends only very weakly on the contact angle over a relatively large range. Furthermore, we assume that the flow is two-dimensional (ignoring variation in the $y$-direction), since 3D simulations require significant computational resources and comparison of 2D and 3D results for the same system under air at atmospheric conditions showed that the 3D effects are also relatively weak.[3] The 2D system corresponds to the central vertical ($x$-$z$) plane of the test cell.

Initially, the fluid is stationary with uniform temperature $T_0 = (T_c + T_h)/2$ (we set $T_0 = 293$ K in all cases), the liquid layer is of uniform thickness $d_l = 2.5$ mm (such that the liquid-gas interface is flat), and the gas layer is a uniform mixture of the vapor and the air. The partial pressure of the vapor $p_v = p_s(T_0)$ is set equal to the saturation pressure at $T_0$, $p_s(T_0) \approx 4.3$ kPa, calculated from (12). The partial pressure of air $p_a$ was used as a control parameter, which determines the net mass of air in the cavity. As the system evolves towards an asymptotic state, the flow develops in both phases and the gradients in the temperature and vapor concentration are established. The simulations are first performed on a coarse hexahedral mesh (initially all cells are cubic with a dimension of 0.5 mm), since the initial transient state is of secondary interest. Once the transient dynamics have died down, the simulations are continued after the mesh is refined in several steps, until the results become mesh independent.

In order to investigate the effect of noncondensables on the the flow, we performed numerical simulations with the average concentration of air $\bar{c}_a$ ranging from to 0% (pure vapor) to 96% (atmospheric pressure), and the temperature difference $\Delta T$ ranging from 2 K to 30 K. As a reference, in the experiments of Li *et al.*[1] the concentration of air varied betwen 11% and 96% and $\Delta T$ – from 0.9 K to 12.5 K.

### A. Convection under Atmospheric Conditions

We have already investigated convection under atmospheric conditions (with a contact angle $\theta = 50°$). In qualitative agreement with experiments, we found the flow to develop a convection pattern as $\Delta T$ was increased, with the flow becoming unsteady above $\Delta T = 20$ K.[3] For the contact angle $\theta = 90°$ considered here the results are essentially the same, as streamlines of the flow shown in Fig. 2 illustrate. For $\Delta T \lesssim 3$ K we find a steady flow featuring one large convection cell spanning almost the entire horizontal extent of the liquid layer, and a small convection roll next to the hot wall. Following Riley and Neitzel's terminology,[7] this flow is referred to as steady unicellular flow (SUF). As $\Delta T$ is increased to $\Delta T = 4$ K, a new convection cell nucleates near the hot wall. As $\Delta T$ is increased further to 10 K, additional convection cells appear. We call this regime partial multicellular flow (PMC) following the terminology from Li *et al.*[1] At $\Delta T$ is raised to 20 K, convection cells spread across the entire horizontal extent of the liquid layer; this state is referred to as steady multicellular flow (SMC). The wavelength of the convective pattern is found to increase monotonically with $\Delta T$ (in contrast, the number of convection cells increases in PMC and decreases in SMC). Finally, at $\Delta T = 30$ K the flow becomes unsteady (not shown); this state is referred to as oscillatory multicellular flow (OMC). These trends are consistent with experiments of Riley and Neitzel[7] and Li *et al.*[1] and with numerical simulations of Shevtsova *et al.*[11] Riley and Neitzel did not distinguish between PMC and SMC, but from the discussion in Ref.[7] it appears that transition between SUF and SMC in their study actually corresponds to the transition between SUF and PMC in our terminology.

The flow in the gas layer mostly mirrors the flow in the liquid layer, with weaker (clockwise) convection

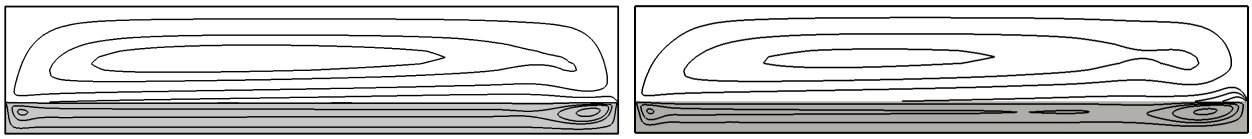

$\Delta T = 10$ K $\Delta T = 20$ K

**Figure 3. Flow patterns for $\bar{c}_a = 0.16$.**

cells located directly above the (counterclockwise) convection cells in the liquid layer. This is not surprising, since convection in both layers is predominantly driven by the modulation of thermocapillary stresses along the free surface. Furthermore, we find two (counterclockwise) convection cells in the top-left and top-right corners of the cavity, where buoyancy in the gas layer dominates.

### B. Convection at Reduced Concentration of Air

Most of the passive evaporative cooling devices such as heat pipes and thermosyphons are operated in the near absence of noncondensable, when most but not all of the air is evacuated. In order to investigate the effect of small amounts of noncondensables on the the flow, we performed a series of numerical simulations with average concentrations of air $\bar{c}_a$ taking values of 0%, 1%, 4%, 6%, 8%, and 16% at temperature differences $\Delta T$ as high as 30 K.

A reduction in the average concentration of air from 96% ($\bar{c}_a = 0.96$, $p_a \approx 101$ kPa) to 16% ($\bar{c}_a = 0.16$, $p_a \approx 0.7$ kPa) does not appreciably change the flow patterns themselves, however it does lead to a substantial increase in the values of $\Delta T$ at which transitions between different convection patterns take place. For instance, as Fig. 3 shows, the temperature at which the first additional convection cell appears increases almost five-fold, to $\Delta T \approx 20$ K, compared with the value at atmospheric conditions. We find neither steady nor oscillatory multicellular convection patterns even as $\Delta T$ increases past 30 K.

The unicellular flow is very similar in the two cases: the streamlines of the flow remain horizontal in the central portion of the liquid layer, indicating that velocity is horizontal, with the vertical profile that is independent of the position $x$ (as well as the concentration $\bar{c}_a$). This is consistent with a flow which is primarily driven by thermocapillary stresses and buoyancy only playing a minor role. Near the end walls the flow velocity at the free surface exhibits slight dependence on the concentration, which can be seen by comparing the spacing between streamlines in the gas phase. At atmospheric conditions the flow is slighly faster near the hot wall, while at $\bar{c}_a = 0.16$ the flow is slightly faster near the cold wall.

A further decrease in the average concentration $\bar{c}_a$ suppresses convective patterns even more. As Fig. 4 illustrates, at $\bar{c}_a = 0.01$ (1% air) the flow structure remains qualitatively similar for all $\Delta T \leq 30$ K, i.e., transitions between different convection patterns disappear completely. Just like in the case of steady unicellular flow at higher $\bar{c}_a$ we find two convection cells in the liquid layer (so we classify this as a steady unicellular flow), however the shape of both convection cells has changed. The flow is much faster near the end walls than in the middle portion of the liquid layer, which suggests that thermocapillarity at $\bar{c}_a = 0.01$ is substantially reduced compared with the case of $\bar{c}_a = 0.16$ and buoyancy is becoming progressively more important, especially near the end walls.

Another major difference with the $\bar{c}_a = 0.16$ case is found by comparing the flow fields in the gas. While at higher concentrations of air the flow pattern is dominated by clockwise recirculation, at lower concentrations of air the flow becomes essentially unidirectional, with vapor flowing from the region of intense evaporation

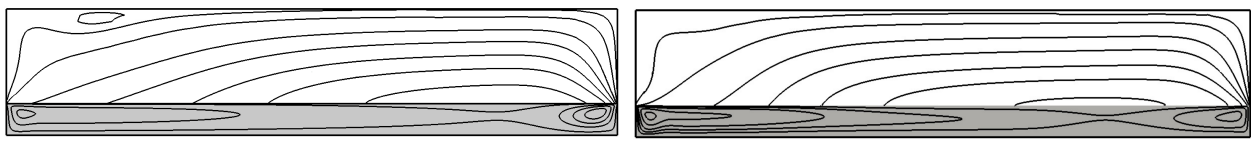

$\Delta T = 10$ K $\Delta T = 30$ K

**Figure 4. Flow patterns at $\bar{c}_a = 0.01$.**

near the hot wall to the region of intense condensation near the cold wall, presumably sweeping much of the air towards the cold wall and making the concentration profile noticeably asymmetric.

In fact, the flow in both phases at $\bar{c}_a = 0.01$ is qualitatively very similar to the flow found at $\bar{c}_a = 0$ (when air is completely absent), as Fig. 5 illustrates. We have shown previously[3] that in the latter case thermocapillary stresses vanish almost entirely, so the flow is driven primarily by buoyancy. In the former case, the presence of air, despite its low concentration, is sufficient to generate thermocapillary flow in the central portion of the cavity that is comparable in strength to that generated by buoyancy.

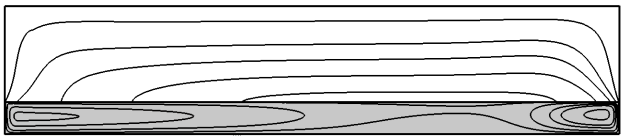

**Figure 5. Flow pattern in the absence of air at $\Delta T =$ 10 K.**

### C. Discussion

Although in the previous section we have only presented the flow patterns for the most typical cases, all our numerical results (a total of almost two dozen independent simulations) are summarized in Table 2 as a function of the average concentration of air $\bar{c}_a$ and the imposed temperature difference $\Delta T$. We find that all transition thresholds increase as the concentration of noncondensables is decreased. In particular, the steady unicellular flow that is only found for $\Delta T \lesssim 3$ K at atmospheric conditions is found for all $\Delta T$ considered here for $\bar{c}_a \leq 0.08$. Other regimes, such as partial multicellular flow or the steady multicellular flow are only found at higher concentrations of noncondensables and oscillatory multicellular convection is only found at atmospheric conditions.

State diagrams are typically presented in terms of nondimensional parameters, such as the interfacial Marangoni number

$$Ma = \frac{\gamma d_l^2 \Delta T}{\mu_l \alpha_l L} \tag{26}$$

characterizing thermocapillarity and the Rayleigh number

$$Ra = \frac{\beta_l \rho_l g d_l^4 \Delta T}{\mu_l \alpha_l L} \tag{27}$$

characterizing buoyancy or, alternatively, the dynamic Bond number $Bo_D = Ra/Ma$, which are defined in terms of the material properties of the liquid phase and $\Delta T$. However, in this case neither $Ma$ nor $Ra$ serve as useful parameters over the entire range of $\bar{c}_a$. For instance, under atmospheric conditions, $\bar{c}_a = 0.96$, the ratio $\Delta T/L$ which enters the definition of $Ma$ provides a reasonable approximation of the interfacial temperature gradient $\tau$ definining the magnitude of thermocapillary stresses.[3] On the other hand, in the absence of noncondensables, $\bar{c}_a = 0$, thermocapillary stresses essentially vanish and the ratio $\Delta T/L$ overestimates $\tau$ by many orders of magnitude.[17] Our simulations suggest that $Ma$ is a relevant parameter only for $\bar{c}_a \gtrsim 0.08$. Similarly, in the absence of air buoyancy dominates and $Ra$ is a relevant parameter, while at atmospheric conditions buoyancy, at least in the $Bo_D = 0.893$ case considered here, is negligible compared to thermocapillarity.

| $\Delta T$ (K) | $Ra$ | $\bar{c}_a$ | | |
|---|---|---|---|---|
| | | $\leq 0.08$ | 0.16 | 0.96 |
| 2 | 342 | SUF | SUF | SUF |
| 4 | 684 | SUF | SUF | PMC |
| 7 | 1197 | SUF | SUF | PMC |
| 10 | 1710 | SUF | SUF | PMC |
| 15 | 2565 | SUF | SUF | SMC |
| 20 | 3420 | SUF | PMC | SMC |
| 30 | 5129 | SUF | PMC | OMC |

**Table 2. The flow regimes as a function of imposed temperature difference $\Delta T$ and average air concentration $\bar{c}_a$.**

Our results are in good qualitative agreement with the experimental observations of Riley and Neitzel,[7] Villers and Platten,[4] and Li *et al.*[1] In particular, the convection patterns found at atmospheric conditions agree very well with experimental observations. The numerically computed flow patterns also agree well with flow visualizations performed by Li *et al.*[1] who also investigated convection at reduced concentrations of noncondensables ($\bar{c}_a = 0.11, 0.34, 0.56$). Over that range, they found the same trends as we did: the transitions between different regimes are delayed as the concentration of noncondensables is reduced.

The values of $\Delta T$ at which the transitions happen in the numerics cannot be compared directly with experiments of Riley and Neitzel[7] and Villers and Platten[4] who used different working fluids (acetone and higher viscosity silicone oil, respectively). However, there are noticeable discrepancies even with the experiments of Li *et al.*[1] which used the same working fluid. For instance, in the experiment, at atmospheric conditions, transition from SUF to PMC happens at $\Delta T \approx 2$ K, transition from PMC to SMC – at $\Delta T \approx 3$ K, and transition from SMC to OMC – at $\Delta T \approx 8$ K. These discrepancies can be attributed to a number

of differences between the numerical simulations and the experiments. For instance, 2D simulations do not capture the effects of strong lateral confinement (3D effects) characterizing the experiment. The differences in the contact angle also affect the results. Furthermore, although our intent was to match the experimental conditions as best we could, some material parameters reported in the literature (and used in the numerics) turned out to be substantially different from those measured in the experiment. For instance, the Prandtl number reported in the experimental study is 9.2 as opposed to 6.8 used in the numerics. The value of the Bond number was also substantially different ($\sim 0.7$ in the experiment vs. $\sim 0.9$ in the numerics).

## IV. Conclusions

We have developed, implemented, and validated a comprehensive numerical model of two-phase flows of confined volatile fluids, which accounts for momentum, mass, and heat transport in both phases and phase change at the interface. This model was used to investigate how the presence of noncondensable gases such as air affects buoyancy-thermocapillary convection in a layer of volatile liquid confined inside a sealed cavity subject to a horizontal temperature gradient.

The presence of noncondensables was found to have a profound effect on the heat and mass transfer. The numerical results show that the convection pattern in the liquid layer can undergo substantial changes as the concentration of air in the vapor space is varied. Moreover, the transition thresholds between different flow regimes also change significantly with the concentration of air. At atmospheric conditions, the flow transitions from steady unicellular flow, to partial multicellular to steady multicellular flow, and eventually to oscillatory multicellular flow. The transitions are delayed as the concentration of air decreases, and disappear completely at concentrations of order 8%. For lower concentrations only unicellular flow is observed.

Rather expectedly, noncondensables were found to have a significant effect on the flow even at very low concentrations. In fact we observed qualitative and quantitative changes at air concentration of only a few percent. In comparison, the lowest value of the concentration that could be reached in experiments of Li *et al.*[1] was considerably higher, around 11%. As we mentioned previously, in order to enhance phase change and the associated heat transfer in sealed thermal management devices, most of the noncondensables is removed from their interior. This likely brings the typical concentrations inside those devices down to values in the range of 5% to 20%, where the effect of noncondensables on the flow of mass and heat most definitely cannot be ignored.

## Acknowledgments

This work has been supported by ONR under Grant No. N00014-09-1-0298. We are grateful to Zeljko Tukovic and Hrvoje Jasak for help with numerical implementation using OpenFOAM.

## References

[1]Li, Y., Grigoriev, R. O., and Yoda, M., "Experimental study of the effect of noncondensables on buoyancy-thermocapillary convection in a volatile silicone oil," *Phys. Fluids*, 2013, pp. under consideration.

[2]Faghri, A., *Heat Pipe Science And Technology*, Taylor & Francis Group, Boca Raton, 1995.

[3]Qin, T., Željko Tuković, and Grigoriev, R. O., "Buoyancy-thermocapillary convection of volatile fluids under atmospheric conditions," *Int. J Heat Mass Transf.*, 2014, pp. accepted for publication.

[4]Villers, D. and Platten, J. K., "Coupled buoyancy and Marangoni convection in acetone: experiments and comparison with numerical simulations," *J. Fluid Mech.*, Vol. 234, 1992, pp. 487–510.

[5]De Saedeleer, C., Garcimartín, A., Chavepeyer, G., Platten, J. K., and Lebon, G., "The instability of a liquid layer heated from the side when the upper surface is open to air," *Phys. Fluids*, Vol. 8, No. 3, 1996, pp. 670–676.

[6]Garcimartín, A., Mukolobwiez, N., and Daviaud, F., "Origin of waves in surface-tension-driven convection," *Phys. Rev. E*, Vol. 56, No. 2, 1997, pp. 1699–1705.

[7]Riley, R. J. and Neitzel, G. P., "Instability of thermocapillarybuoyancy convection in shallow layers. Part 1. Characterization of steady and oscillatory instabilities," *J. Fluid Mech.*, Vol. 359, 1998, pp. 143–164.

[8]Ben Hadid, H. and Roux, B., "Buoyancy- and thermocapillary-driven flows in differentially heated cavities for low-Prandtl-number fluids," *J. Fluid Mech.*, Vol. 235, 1992, pp. 1–36.

[9]Mundrane, M. and Zebib, A., "Oscillatory buoyant thermocapillary flow," *Phys. Fluids*, Vol. 6, No. 10, 1994, pp. 3294–3306.

[10]Lu, X. and Zhuang, L., "Numerical study of buoyancy- and thermocapillary-driven flows in a cavity," *Acta Mech Sinica (English Series)*, Vol. 14, No. 2, 1998, pp. 130–138.

[11]Shevtsova, V. M., Nepomnyashchy, A. A., and Legros, J. C., "Thermocapillary-buoyancy convection in a shallow cavity heated from the side," *Phys. Rev. E*, Vol. 67, 2003.

[12]Zhang, J., Watson, S. J., and Wong, H., "Fluid Flow and Heat Transfer in a Dual-Wet Micro Heat Pipe," *J. Fluid Mech.*, Vol. 589, 2007, pp. 1–31.

[13]Kuznetzov, G. V. and Sitnikov, A. E., "Numerical Modeling of Heat and Mass Transfer in a Low-Temperature Heat Pipe," *Journal of Engineering Physics and Thermophysics*, Vol. 75, 2002, pp. 840–848.

[14]Kaya, T. and Goldak, J., "Three-Dimensional Numerical Analysis of Heat and Mass Transfer in Heat Pipes," *Heat Mass Transfer*, Vol. 43, 2007, pp. 775–785.

[15]Kafeel, K. and Turan, A., "Axi-symmetric Simulation of a Two Phase Vertical Thermosyphon using Eulerian Two-Fluid Methodology," *Heat Mass Transfer*, Vol. 49, 2013, pp. 1089–1099.

[16]Fadhl, B., Wrobel, L. C., and Jouhara, H., "Numerical Modelling of the Temperature Distribution in a Two-Phase Closed Thermosyphon," *Applied Thermal Engineering*, Vol. 60, 2013, pp. 122–131.

[17]Qin, T., Željko Tuković, and Grigoriev, R. O., "Buoyancy-thermocapillary convection of volatile fluids their vapors," *Int. J Heat Mass Transf.*, 2014, pp. under review.

[18]Schrage, R. W., *A Theoretical Study of Interface Mass Transfer*, Columbia University Press, New York, 1953.

[19]Wayner, P. J., Kao, Y. K., and LaCroix, L. V., "The Interline heat transfer coefficient of an evaporating wetting film," *Int. J. Heat Mass Transfer*, Vol. 19, 1976, pp. 487–492.

[20]Wang, H., Pan, Z., and Garimella, S. V., "Numerical investigation of heat and mass transfer from an evaporating meniscus in a heated open groove," *Int. J. Heat Mass Transfer*, Vol. 54, 2011, pp. 30153023.

[21]`http://www.openfoam.com`, 2012.